ilmedia

Technische Universität Ilmenau

Lenk, Leonhard; Mitschunas, Beate; Sinzinger, Stefan

Design method for zoom systems based on tunable lenses

Design method for zoom systems based on tunable lenses

Leonhard Lenk,* Beate Mitschunas, and Stefan Sinzinger
Technische Universität Ilmenau, Fakultät für Maschinenbau, Technische Optik, Ilmenau,
Germany

Abstract. It is well known that tunable lenses, with refractive power that can be varied, e.g., by changing the curvature of a membrane, can replace the motion of lens groups in zoom systems. Similar to classical zoom systems, the performance of these systems is heavily influenced by the fundamental first-order layout. Moreover, the first-order layout sets the most important requirements for the employed tunable lenses. In this contribution, we present a method for the analysis of a large number of possible first-order solutions for typical requirements and for the selection of the most promising layouts. The first-order solution space is mapped, allowing the layouts to be automatically filtered and plotted depending on pre-defined characteristics. Ray tracing of the marginal and chief rays combined with the traditional thin lens aberration theory provide efficient estimations of the expected installation space requirements and performance for each first-order layout. Using an example, we demonstrate good agreement between these estimations and the corresponding real lens layout, optimized by commercial raytracing software. The presented design method for zoom systems based on tunable lenses is compared with similar approaches for classical zoom lenses. © *The Authors. Published by SPIE under a Creative Commons Attribution 4.0 International License. Distribution or reproduction of this work in whole or in part requires full attribution of the original publication, including its DOI.* [DOI: 10.1117/1.OE.61.6.065103]

1 Introduction

Zoom lenses provide a variable focal length, while maintaining a constant image position. In classical zoom lenses, this requires a synchronized motion of lens groups along the optical axis, following complex trajectories. This makes both the fabrication and design of these systems challenging and expensive, and it generally leads to systems that are larger and heavier than comparable lenses with a fixed focal length.

A variety of different approaches have been suggested in the literature to enable lenses to tune their refractive power without moving elements along the optical axis.[1–3] These range from fluidic lenses, in which the variation of curvature of the interface between two liquids changes the focal length,[4,5] to over liquid filled membrane lenses[6–8] to refractive and diffractive Alvarez–Lohmann or Moiré lenses.[9–13] Typically, the refractive power range of these elements is limited and inversely proportional to the aperture diameter.

The literature provides numerous designs for zoom lenses in which tunable lenses partly[14,15] or completely[16,17] replace the motion of lens groups. From a broader point of view, including adaptive optical elements such as adaptive mirrors and spatial light modulators, there are even more examples for similar systems, also known under the terms non-mechanical zoom or adaptive optical zoom.[18–21] These designs promise reduced mechanical complexity and installation space, alleviating some of the issues of classical zoom lenses described above. Because these systems combine the potential for real optical zoom with compact packaging sizes, they are most interesting for compact camera systems, e.g., for integrated sensing and imaging solutions as in light detection and ranging systems or cell phone cameras.

Important system characteristics, e.g., the necessary refractive power range of the tunable lenses, are already determined by the first-order layout. To encounter innovative system

---

*Address all correspondence to Leonhard Lenk, leonhard.lenk@tu-ilmenau.de

solutions, it is useful to comprehensively analyze the first-order solution space, as compared with the direct approach starting from a classical zoom lens layout and replacing the motion of the lens groups directly. The aim of our design method is to find first-order layouts that are adapted to the specific requirements of the respective application and the capabilities of the available tunable lenses. Although there is a wide range of literature discussing first-order calculation approaches for zoom lenses based on tunable lenses in detail,[22] the number of studies covering methods for a systematic search for layouts for this kind of zoom systems seems to be quite limited. Unlike other methods for classical zoom lenses,[23–25] our method sets the main focus on mapping the first-order solution space applying traditional thin lens aberration equations. [26,27] This is based on an extension of ideas presented in our earlier work.[26] A similar approach for telescopes consisting of two adaptive mirrors was demonstrated in Ref. [28]. We limit our considerations to zoom lenses with two tunable groups and up to four groups in total. After describing the algorithm and calculation approach of our method, we demonstrate the application to an exemplary set of requirements and compare our design method with other approaches.

2 Method

2.1 Algorithm

The algorithm that forms the backbone of our method can be divided into two main steps (Fig. 1). The first step is performing a scan of the solution space. This is achieved by varying the input parameters for the calculation approach described below, with step sizes and within boundaries that have to be adapted to the respective requirements. Each combination of input parameters yields one possible first-order layout.

The second step is the analysis of this usually quite large number of first-order layouts. This mainly consists in step-wise excluding layouts from consideration, at first based on their first-order properties, subsequently going into a more detailed analysis using additional input parameters. Thereby, the number of layouts under consideration is systematically reduced down to the selection of one or multiple final layouts.

2.2 Calculation Approach

2.2.1 Required equations

The possible first-order layouts for a zoom lens with two tunable groups, without moving groups and up to four groups in total, can be divided into six different variations, depending on the position of the tunable groups (Table 1). We define a group as a number of lenses with small distances between each. This also leads to the important approximation that gives the refractive power of the group as the sum of the refractive powers of the individual lenses, and therefore, the group's refractive power tuning range equals the tuning range of the tunable lens within the group.
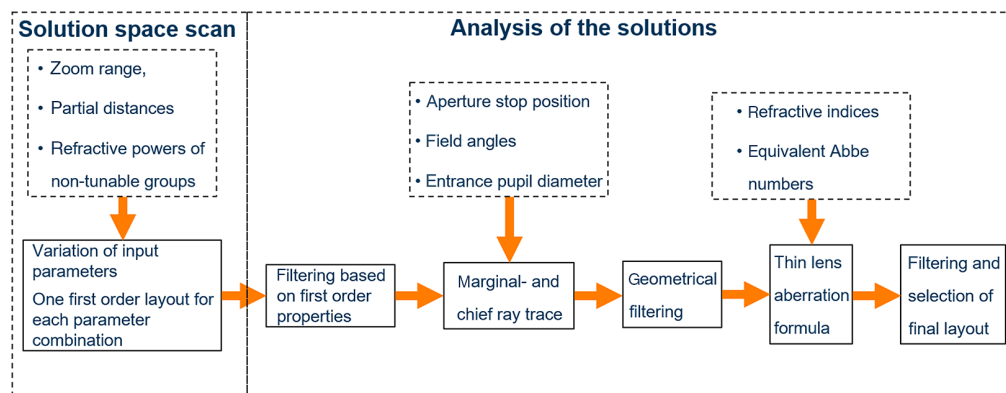

Fig. 1 Overview of the algorithm.

Table 1 Overview of the variations, possible positions of tunable groups (t).

Variation no.	Lens group no.			
	1	2	3	4
1	t	t	—	—
2	t	—	t	—
3	t	—	—	t
4	—	t	t	—
5	—	t	—	t
6	—	—	t	t

The aim is to retrieve all reasonable first-order layouts within given boundaries before analyzing their performance. To access the first-order solution space, a set of equations needs to be derived for each variation that yields the first-order system characteristics over the full zoom range, for a given set of input parameters. According to the usual practice for photographic zoom lenses, we set the object at infinity for all following considerations.

In the following, we describe the calculation approach using variation 3 as an example, in which the first tunable group is the first group of the system, and the second tunable group is group number four (Fig. 2).

We define the refractive power F' of the whole system at any point of the zoom range as a fixed requirement. All of the first-order system characteristics that do not change over the zoom range are defined as variable input parameters, which are the partial distances e'_1, e'_2, e'_3, and e'_4, as well as the refractive powers of the non-tunable groups F'_2 and F'_3. The variation of these six input parameters defines a six dimensional solution space. To find a first-order layout for each combination of these input parameters, two equations need to be derived:

1. One equation for the refractive power of the first tunable lens F'_1 depending on the system's refractive power F', independent of F'_4: $F'_1(F')$ and
2. One equation for the refractive power of the second tunable lens F'_4 depending on F'_1.

The derivation of these equations for variation 3 is described in Appendix A. The derivation of the equations for the remaining variations is performed by describing them as variation 3 systems, with some small changes. All of the resulting equations are shown in Table 2.
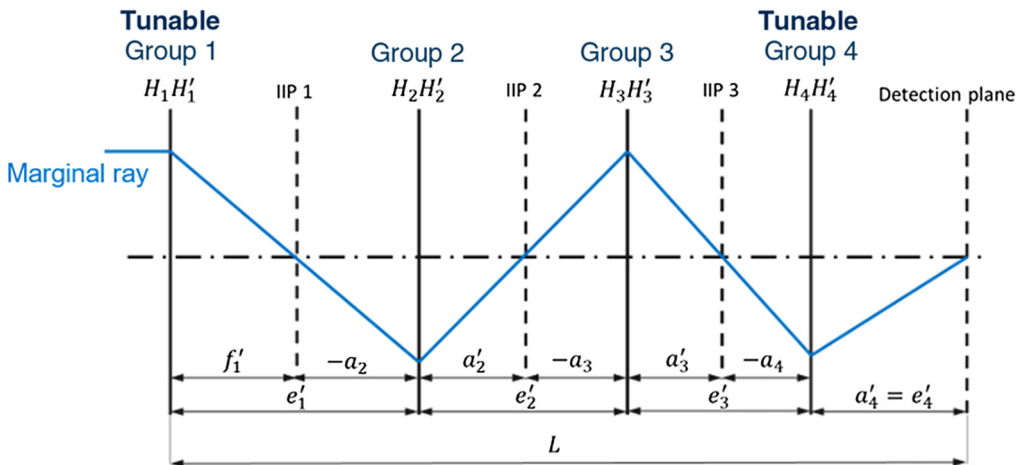

Fig. 2 First-order layout of a variation 3 system.

Table 2 Equations for the tunable groups' refractive powers for all variations.

Variation no.	Equations
1	$F_1'(F') = -\frac{1}{e_1'}\left[F'(1 - e_4' F_4') \left[e_2' + \left(e_3' + \frac{e_4'}{1 - e_4' F_4'} \right)(1 - e_2' F_3') \right] - 1 \right]$
	$F_2'(F_1') = \frac{1}{e_2' + \cfrac{1}{-F_3' - \cfrac{1}{-e_3' - e_4' + \cfrac{e_4'}{1 - \frac{1}{e_4' F_4'}}}}} - \frac{1}{\frac{1}{F_1'} - e_1'}$
2	$F_1'(F') = \frac{F'(e_3'(1 - e_4' F_4') + e_4') - (1 - e_2' F_2')}{-e_1' - e_2'(1 - e_1' F_2')}$
	$F_3'(F_1') = \cfrac{1}{\left(e_3' + \frac{e_4'}{1 - e_4' F_4'} \right)\left[1 - \cfrac{e_3' + \frac{e_4'}{1 - e_4' F_4'}}{\cfrac{\left(\frac{1}{F_1'} - e_1' \right)}{e_2' + e_3' + \frac{1}{1 + \left(\frac{1}{F_1'} - e_1' \right)F_2'}} + \frac{e_4'}{1 - e_4' F_4'}} \right]}$
3	$F_1'(F') = \frac{e_4' F' - (1 - e_3'(F_2' - e_2' F_2' F_3' + F_3') - e_2' F_2')}{-e_1' - e_2'(1 - e_1' F_2') + e_3'(e_1'(F_2' - e_2' F_2' F_3' + F_3') - 1 + e_2' F_3')}$
	$F_4'(F_1') = \cfrac{1}{e_4'\left(1 - \cfrac{e_4'}{e_3' + e_4' - \cfrac{1}{\cfrac{1}{\frac{1}{\frac{1}{F_1'} - e_1'} + F_2'} - e_2'} + F_3'} \right)}$
4	$F_2'(F') = \frac{-F'[e_3'(1 - e_4' F_4') + e_4'] + 1 - (e_1' + e_2')F_1'}{e_2'(1 - e_1' F_1')}$
	$F_3'(F_2') = $ Equation $F_3'(F_1')$ from variation 2
5	$F_2'(F') = \frac{e_4' F' - (1 - e_3' F_3') - F_1'[-e_1' - e_2' + e_3'(e_1' F_3' - 1 + e_2' F_3')]}{F_1'(e_1' e_2' + e_1' e_3' - e_1' e_2' e_3' F_3') - (e_3' - e_2' e_3' F_3' + e_2')}$
	$F_4'(F_2') = $ Equation $F_4'(F_1')$ from variation 3
6	$F_4'(F') = \frac{-F'(e_3' + e_4') + F_1'[-e_1' - e_2'(1 - e_1' F_2')] + (1 - e_2' F_2')}{-F' e_3' e_4'}$
	$F_3'(F_4') = $ Equation $F_3'(F_1')$ from variation 2

2.2.2 Search for extremal values of $F_4'(F_1')$

To understand the behavior of the tunable lenses over the zoom range, it is important to know at which point of the zoom range the tunable lenses will have their maximum or minimum refractive powers. The corresponding analysis is demonstrated in the following only for variation 3, but the same procedure yields the same conclusions for the remaining variations.

$F_1'(F')$ in Table 2 clearly shows monotonic behavior. This means that F_1' will either be strictly non-decreasing or non-increasing when the overall refractive power of the system F' is changing from the beginning to the end of the zoom range. So F_1' will clearly have no extremal values in between the boundary values. Therefore, the next step is a search for extremal values of $F_4'(F_1')$.

At first, we need the first derivative of $F_4'(F_1')$; its derivation is shown in Appendix B. The result is as follows:

$$\frac{\delta F_4'}{\delta F_1'} = -(L_4(F_1') - a_4')^{-2} \cdot ((a_3(F_1'))^{-1} + F_3')^{-2}$$

$$\cdot (a_3(F_1'))^{-2}((a_2(F_1'))^{-1} + F_2')^{-2} \cdot (a_2(F_1'))^{-2}(F_1')^{-2}. \tag{1}$$

From Eq. (1), it is clear that $\frac{\delta F_4'}{\delta F_1'}$ will always be negative because all expressions within brackets are real numbers, the exponent -2 will thus yield positive values, and the negative sign in front of the first bracket determines the negative sign of the whole expression.

From this result, two important conclusions can be drawn:

1. Because the refractive power of the first tunable lens F_1' varies monotonically over the zoom range, there will be no extremal values for F_4' apart from the values at the boundaries, which are the beginning (short focal length) and the end of the zoom range (long focal length). Therefore, it is enough to know the values of the refractive powers of the tunable lenses at the beginning and at the end of the zoom range to calculate the maximum tuning range of the refractive power.

2. The refractive powers of the tunable lenses will always change in opposite directions.

The same results are true for the remaining variations.

2.3 Important Relations for Analysis of the Solutions

2.3.1 General approach

Following the algorithm shown in Fig. 1, the second step of the method is the systematic analysis of the first-order layouts that result from the equations presented above. For a better idea of the geometry and expected behavior of each single system, the on-axis marginal ray and the chief ray for the outermost field point are traced. This requires additional parameters; the most important ones are the position of the aperture stop, the entrance pupil diameter, and the field angle.

The most important characteristics that can be accessed by this procedure are the necessary aperture diameters of the groups, the well-known F-number, and the angle of incidence of the chief ray at the image plane that influences the amount of natural- and pixel vignetting. Additionally, the difference between the chief ray angle before and after the system also influences the amount of distortion. The ratio of aperture diameter and focal length of each group, the so-called relative aperture k_n, can be used to estimate the expected difficulties with aperture related aberrations, e.g., spherical aberration.

Although the first-order layout is a very simplified approximation of the final thick lens system, some aberrations are heavily influenced by system properties that are already determined within the first-order layout. These aberrations are Petzval curvature, axial, and lateral color, which are also called shape independent aberrations, because they are not depending on the shape of the lenses for a system of thin lenses.[29] To take into account the expected aberration behavior of the final system, the following relations based on traditional thin lens theory are used.

2.3.2 Petzval sum

The Petzval curvature is equal to the field curvature if astigmatism is corrected. It is the reciprocal of the Petzval radius r_p, and for a system of thin lenses, it is described by the so-called Petzval sum as follows, with n_n denoting the refractive index of group number n:[30]

$$\frac{1}{r_p} = \sum_{n=1}^{N} \frac{F_n'}{n_n}. \tag{2}$$

2.3.3 Axial color

The axial color for a system of N thin lenses and object at infinity is calculated as[30]

$$\Delta_\lambda s' = -\frac{1}{F'^2} \sum_{n=1}^{N} \left(\frac{h_{mn}}{h_{m1}}\right)^2 \frac{F_n'}{\nu_n}, \tag{3}$$

where h_{mn} denotes the marginal ray height at thin lens number n, and ν_n denotes its Abbe number.

2.3.4 *Lateral color*

The equation for lateral color of a system of thin lenses is as follows:[30]

$$\frac{\Delta_\lambda y'}{y'} = c \cdot \sum_{n=1}^{N} \frac{h_{mn}}{h_{m1}} \frac{h_{pn}}{h_{p1}} \frac{F'_n}{\nu_n}. \tag{4}$$

Here, h_{pn} denotes the chief ray height at thin lens number n, and y' is the object height. The factor c describes the position of the entrance pupil in relation to the first group of the system and the object and depends on the position of the aperture stop within the system. The respective expressions for aperture stop positions in the first three groups are given in Appendix C.

2.3.5 *Handling of material properties*

Like the Petzval sum, both lateral and axial color depend on the choice of material, in this case represented by the Abbe number. Because the choice of materials for the tunable lenses is usually quite limited, the refractive index and Abbe number cannot be estimated independently of each other for the tunable groups. However, for the non-tunable groups, there are materials available with different refractive indices and the same Abbe number. Moreover, the equivalent Abbe number of one group can be varied in a wide range using doublets or triplets. Therefore, it should be possible to treat the choice of effective refractive index of a non-tunable group independent of the equivalent Abbe number, at least to some extent. This can be used to independently balance both Petzval sum and the color aberrations.

As opposed to that, axial and lateral color have to be regarded together when searching for the best combination of Abbe numbers. At this point, it is worth noting that, according to Ref. 29, it is only possible to have both the axial and lateral color corrected for a system of several groups if the groups themselves are corrected for axial color. This poses a challenge for a lens with tunable groups containing only one tunable lens, in particular membrane or fluidic lenses, because they usually cannot be achromatized over the whole tuning range. For such systems, the aim must be to reduce the residual color aberration as far as possible.

2.4 *Implementation in MATLAB®*

Object-oriented programming is well suited to implementing the algorithm described above (Fig. 1).[31] A class "variation X" (with X being the respective number of the zoom lens variations in Table 1) is defined. All of the parameters necessary to describe a specific first-order layout of the respective variation are defined as properties of the class, e.g., the partial distances of the groups and their refractive powers. The constructor of the class uses the equations derived above to calculate the refractive powers of the tunable lenses at the beginning and at the end of the zoom range. The input parameters, as well as the calculated refractive powers are used to set the values of the object's properties. Thereby, a specific first-order layout within the possible solution space is created as an object of class variation X.

To scan a certain region of the solution space, the input parameters of the calculation approach are varied within chosen boundaries using a loop. Each cycle of the loop creates one object of the class variation X using one set of input parameter values. The created objects are saved within an array. This scanning process is performed by the first main MATLAB®-script called CalcAppVX.m (Fig. 3).

All relations for the analysis of the solutions described above are implemented as functions in MATLAB®. These functions are generally designed to accept whole arrays of variation X objects as input variables, as well as the respective additional input variables, e.g., the position of the aperture stop. This allows for efficient processing of large amounts of data using vectorization, i.e., the simultaneous application of operations to all elements of an array. The functions create additional arrays, which contain the resulting value for each first-order system in the object array. Each first-order layout is connected to the respective result of the function by the index within the arrays (Fig. 4).
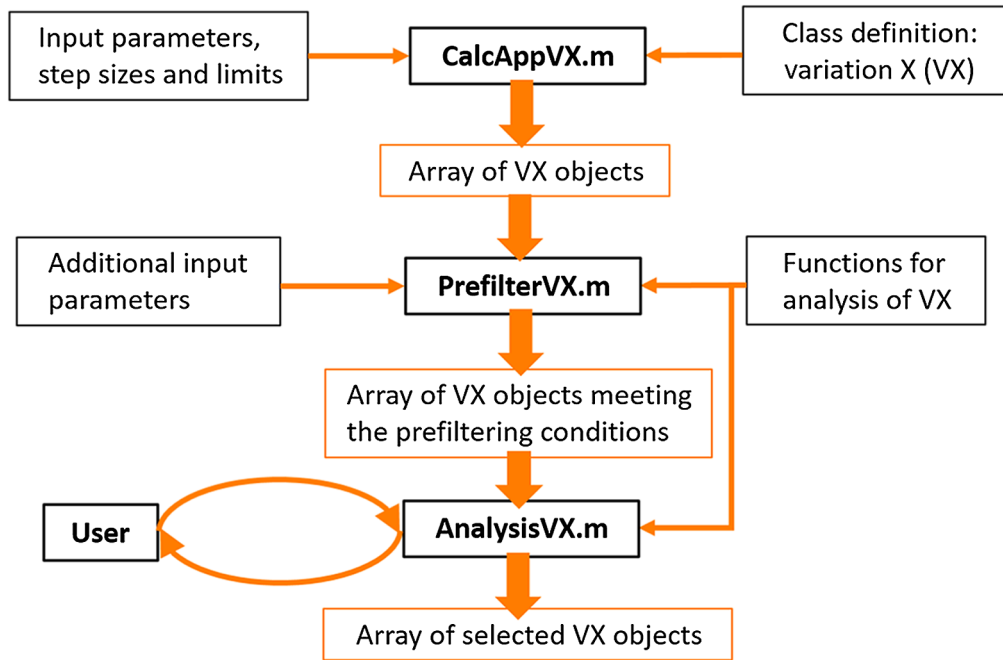
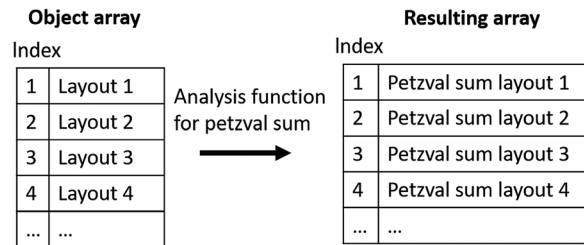**Fig. 3** Structure of the implementation in MATLAB®.

Fig. 4 Using array indexing for efficient addressing of analysis results.

Therefore, it is easily possible to plot the layouts depending on various properties. It is also possible to filter the layouts by selecting only the elements of the object array with indices that equal the indices of elements within the resulting array that meet certain conditions. This is used by the second and the third main MATLAB®-script (Fig. 3), which implements the analysis of the solutions shown in the general algorithm (Fig. 1). The script PrefilterVX.m performs an automated filtering of the objects, and the script AnalysisVX.m is meant for the more detailed, user defined step by step-filtering of the remaining objects.

3 Demonstration

In the following, the design method is applied to a somewhat unusual example of a three group tele zoom lens for a 4/3'' sensor. Usual examples of zoom lens designs based on tunable lenses are limited to much smaller sensor formats (e.g., below 1/2.8''[14–17]). The aim is to find first-order layouts with requirements that can be met by current tunable lenses.

3.1 *Preparations*

The limits of current tunable lenses in the necessary dimensions seem to be lying at a tuning range of -18 to 18 dpt and diameters of 20 mm (e.g., the membrane lens ML-20-37 by

Table 3 Chosen requirements for the desired zoom lens based on tunable lenses. Typical pixel sizes taken from Ref. 35.

General			
Zoom range		$f' = 35$ mm$\ldots 70$ mm	
f-number		$F\# = 4.0\ldots 5.0$	
Total track		$L_{\text{first order}} \leq 100$ mm; $L_{\text{real lens}} \leq 120$ mm	
Chief ray angle at sensor		$w' \leq 15$ deg	
Tunable lenses			
Aperture diameter		$D_{\text{tune}} \leq 20$ mm	
Refractive power range		$|\Delta F'_n| \leq 34$ dpt	
Sensor/ resolution	MP	Pixel size (μm)	Nyquist frequency $\left[\frac{lp}{mm}\right]$
Number of pixels	10	4.7	107
	12	4.3	117
	16	3.75	134
	20	3.3	152
MTF		MTF $\geq$ 50% at 0.5 Nyquist; MTF $\geq$ 20% at Nyquist	

Optotune[7]). To our knowledge, no designs for zoom lenses based on tunable lenses exist for sensor formats as large as 4/3''. Therefore, commercial zoom lenses, based on classical zoom principles, are used to derive realistic requirements for the lens.

Considering the fairly limited aperture diameters of the tunable lenses, a system for the tele-range seems most appropriate because typically wide-angle lenses require quite large diameters for the first lens group. One example for these is Panasonic's LUMIX G VARIO 35-100 mm F4.0-5.6 ASPH. MEGA O.I.S. with a total length ranging from 50 to 78 mm.[32] One example for a four third digital single-lens reflex camera is the Olympus E-450 from the year 2009, at 10 MP (mega pixels).[33] Typical pixel numbers for mirrorless micro four third cameras seem to range from 12 MP for cameras from the years 2008 – 2009, over 16 MP and up to 20 MP for more recent cameras.[34] To reduce the challenge, the requirement for the zoom ratio for the zoom lens based on tunable lenses is set to 2× (focal length 35 to 70 mm) instead of the 3× of the classical system. Preliminary investigations show that the combination of limited aperture diameters (20 mm) and large sensors (sensor diagonal 21.63 mm), as well as the limited refractive power tuning range (−18 to 18 dpt) of the tunable lenses, otherwise leads to a very small number of possible solutions. For comparison, the smaller tunable lens in the system with a large zoom range of 8×, proposed in Ref. 17, has a diameter of 6 mm with a sensor diagonal of 3.6 mm (1/5'') and a necessary tuning range of −84 to 84 dpt. The chosen set of requirements is shown in Table 3.

3.2 Selection of the First-order Layout

3.2.1 Possible variations

As shown in the algorithm (Fig. 1), the first step is a scan of the first-order solution space by variation of the input parameters of the calculation approach. For a three group system, only three different variations have to be considered. These can be described as special cases of the six variations, which were discussed for four group systems (Table 1). Table 4 gives the variations described as the variation 1, variation 4, and variation 2 systems with the refractive power of group 4, as well as the fourth partial distance set to zero.

Table 4 Possible variations of a three group zoom lens with two tunable groups.

	Lens group no.		
Variation	1	2	3
1	t	t	—
4	—	t	t
2	t	—	t

In this way, the calculation approach and all of the equations for analysis can be adapted to systems with less than four groups.

3.2.2 Input parameters for the algorithm

According to our calculation approach, the variable input parameters are the partial distances between the groups e'_1, e'_2, and e'_3, as well as the refractive powers of the non-tunable group F'_{non-t}. For these, it is important to set reasonable limits and step sizes, keeping geometry and the number of resulting combinations in mind. The step size for the refractive power of the non-tunable group is adapted to the absolute value of the refractive power. Thereby, both too large equivalent focal length steps for low refractive powers and unnecessary small equivalent focal length steps for high refractive powers can be avoided (Fig. 5). The limits and step sizes of the variable input parameters are summarized in Table 5.

3.2.3 Automatic prefiltering

The limits and step sizes in Table 5 lead to 3,571,712 theoretically possible combinations of input parameters per variation. To reduce this number, an automatic prefiltering of the solutions is performed. For this, suitable values for the additional input parameters need to be chosen. The position of the aperture stop in all three groups is considered, and the diameter of the entrance pupil at the beginning of the zoom range is calculated from the desired f-number range. The f-number range from $F\#_B = 4$ at the beginning of the zoom range and $F\#_E = 5$ at the end of the zoom range give us the minimum entrance pupil diameters at the beginning $D_{\text{EPB min}} = 8.75$ mm and at the end of the zoom range $D_{\text{EPE min}} = 14$ mm, respectively. Because the diameter of the aperture stop is assumed constant over the zoom range, only systems with an entrance pupil diameter that varies over the zoom range can have an entrance pupil diameter of $D_{\text{EPB}} = D_{\text{EPB min}} = 8.75$ mm. The others need to provide 14 mm. The object space
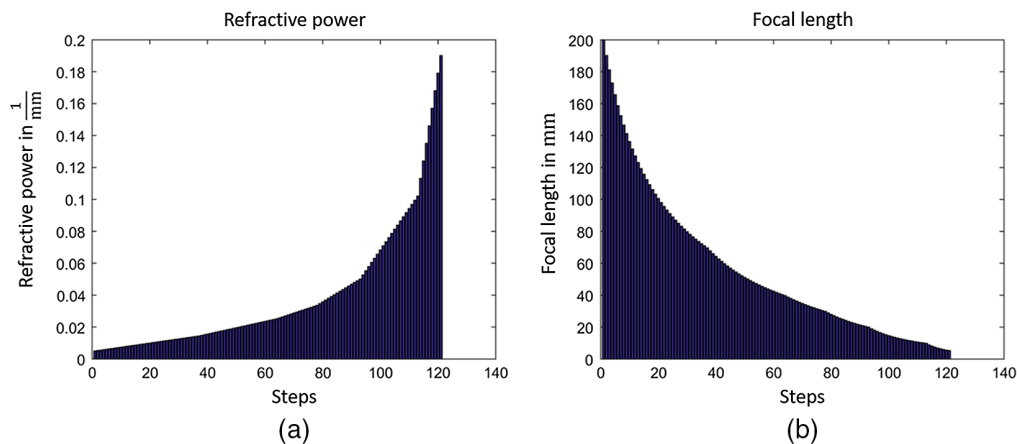

Fig. 5 (a) Refractive power steps and (b) resulting focal length steps.

Table 5 Variable input parameters with respective limits and step sizes.

Parameter	Minimum	Maximum	Step size
e'_1	10 mm	74 mm	2 mm
e'_2	10 mm	74 mm	2 mm
e'_3	16 mm	80 mm	2 mm
$\lvert F'_{\text{non}-t} \rvert$	5 dpt	100 dpt	$\lvert f'_{\text{non}-t} \rvert \geq 70$ mm: 0.26 dpt
			$\lvert f'_{\text{non}-t} \rvert \geq 40$ mm: 0.40 dpt
			$\lvert f'_{\text{non}-t} \rvert \geq 30$ mm: 0.60 dpt
			$\lvert f'_{\text{non}-t} \rvert \geq 20$ mm: 1.10 dpt
			$\lvert f'_{\text{non}-t} \rvert \geq 10$ mm: 2.60 dpt

Table 6 Criteria for automatic prefiltering.

Criterion	Symbol	Limit
Total track	L	≤ 100 mm
Aperture diameters	D_{tunable}	≤ 20 mm
	$D_{\text{non}-\text{tunable}}$	≤ 50 mm
f-number at the end of the zoom range	$F\#_E$	≤ 5.0
Image space chief ray angle	$\lvert w' \rvert$	≤ 15 deg
Relative apertures	k_n	≤ 3
Refractive power tuning ranges	$\lvert \Delta F'_n \rvert$	≤ 34 dpt
Refractive powers	F'_n	≤ 100 dpt

field angle at the beginning $w_B = 17.17$ deg and at the end of the zoom range $w_E = 8.78$ deg are defined by the sensor size and the respective focal lengths. The acceptable amount of vignetting is set to 50% of the height between marginal and chief rays of the beam for the outmost field. With these additional input parameters, the first-order layouts are filtered according to the criteria shown in Table 6.

An overview of the solutions after automatic prefiltering, including the ranges of some important system characteristics, is given in Fig. 6.

Figure 6 shows that some combinations of tunable lens position (i.e., some variations) and aperture stop positions do not yield any first-order layouts that meet the requirements stated above. It is interesting to note that for all remaining layouts the total track L does not go below 64 mm, so it is not possible to create a very compact system under the given circumstances. Looking at the most important characteristic, the required refractive power range for the tunable groups, variation 3, with the aperture stop within group 2, contains layouts with the lowest requirements. Therefore, the following considerations will focus on this part of the solution space.

3.2.4 *"Manual" analysis of the variation 3 layouts with aperture stop in group 2*

After strongly reducing the number of considered first-order layouts, a more detailed analysis and filtering can be performed. For this, it is useful to plot the first-order layouts depending on different characteristics to get a good understanding of the limitations and correlations between them. Subsequently, the remaining solutions can be filtered according to additional requirements to find the most promising layouts.
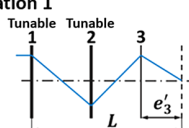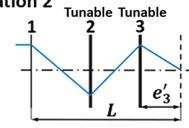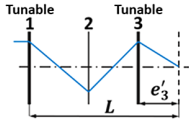
	Aperture stop in group	Number of layouts	Characteristics
Variation 1	1	0	-
	2	117,668	$\lvert\Delta F_1'\rvert = (28.11 \dots 34)\mathrm{dpt}$ $\lvert\Delta F_2'\rvert = (11.84 \dots 34)\mathrm{dpt}$ $L = (64 \dots 100)\mathrm{mm}$ $e_3' = (16 \dots 68)\mathrm{mm}$
	3	0	-
Variation 2	1	0	-
	2	0	-
	3	13,649	$\lvert\Delta F_2'\rvert = (27.84 \dots 34)\mathrm{dpt}$ $\lvert\Delta F_3'\rvert = (12.73 \dots 34)\mathrm{dpt}$ $L = (74 \dots 100)\mathrm{mm}$ $e_3' = (42 \dots 64)\mathrm{mm}$
Variation 3	1	0	-
	2	89,531	$\lvert\Delta F_1'\rvert = (14.28 \dots 34)\mathrm{dpt}$ $\lvert\Delta F_3'\rvert = (8.631 \dots 34)\mathrm{dpt}$ $L = (70 \dots 100)\mathrm{mm}$ $e_3' = (34 \dots 76)\mathrm{mm}$
	3	59,136	$\lvert\Delta F_1'\rvert = (28.11 \dots 34)\mathrm{dpt}$ $\lvert\Delta F_3'\rvert = (12.08 \dots 34)\mathrm{dpt}$ $L = (66 \dots 100)\mathrm{mm}$ $e_3' = (46 \dots 76)\mathrm{mm}$

Fig. 6 Remaining first-order layouts after automatic prefiltering.

The plot of the refractive power ranges of the tunable groups in Fig. 7(a) shows that there are layouts with low tuning range requirements for both tunable groups. Because the difficulties in correcting aberrations for the final system are connected to these refractive power ranges, the first manual filtering step is the selection of the systems with $\lvert\Delta F_n'\rvert \leq 20$ dpt. This reduces the number of layouts under consideration to 22,598.

Although a small incidence angle of the chief ray at the sensor is advantageous for the prevention of natural—and pixel vignetting, the plot in Fig. 7(b) shows that smaller angles also mean larger image distances. Because larger image distances tend to increase the total track and make correction of field dependent aberrations, such as distortion, more difficult, no filtering is applied here. Considering distortion, it is advantageous that the sign of the chief ray angle in the image space equals the positive sign of the chief ray angle in the object space for all remaining layouts.

For the evaluation of the expected Petzval curvature in Fig. 7(c), the values for the refractive indices of the tunable groups are estimated at 1.3, orienting on typical values for optical liquids used in membrane lenses (Table 7). For the non-tunable groups, a value of 1.6 proved to be reasonable. Having layouts close to the zero Petzval curvature for the beginning and end of the zoom range leads to the second manual filtering step: only layouts with a maximum absolute Petzval curvature of 0.01 $\frac{1}{\mathrm{mm}}$ are considered further, reducing the number of layouts to 4070.

As mentioned before, axial and lateral color have to be considered simultaneously because both depend on the equivalent Abbe numbers of the groups ν_1, ν_2, and ν_3. Furthermore, reasonable estimations for the equivalent Abbe numbers, especially of the non-tunable groups, are very difficult. The possible values range from negative values for overcorrected groups, over infinity for corrected groups, to very small positive values for strongly undercorrected groups. To solve this highly multidimensional problem, a simple merit function is used; it contains the contributions to axial and lateral color at the beginning and end of the zoom range (respectively, $\Delta_\lambda s_A'$, $\Delta_\lambda s_E'$, $\frac{\Delta_\lambda y_A'}{y'}$, and $\frac{\Delta_\lambda y_E'}{y'}$), weighted by a weighting factor (respectively, W_{axA}, W_{axE}, W_{latA}, and W_{latE}) Eq. (5).

$$
\begin{aligned}
\mathrm{Merit} = {} & \frac{1}{W_{axA} + W_{axE} + W_{ax\mathrm{Diff}} + W_{latA} + W_{latE} + W_{lat\mathrm{Diff}}} \\
& \cdot \left[W_{axA} \cdot \Delta_\lambda s_A' + W_{axE} \cdot \Delta_\lambda s_E' + W_{ax\mathrm{Diff}} \cdot \lvert \Delta_\lambda s_E' - \Delta_\lambda s_A' \rvert + W_{latA} \right. \\
& \left. \cdot \frac{\Delta_\lambda y_A'}{y'} + W_{latE} \cdot \frac{\Delta_\lambda y_E'}{y'} + W_{lat\mathrm{Diff}} \cdot \left\lvert \frac{\Delta_\lambda y_E'}{y'} - \frac{\Delta_\lambda y_A'}{y'} \right\rvert \right] \cdot
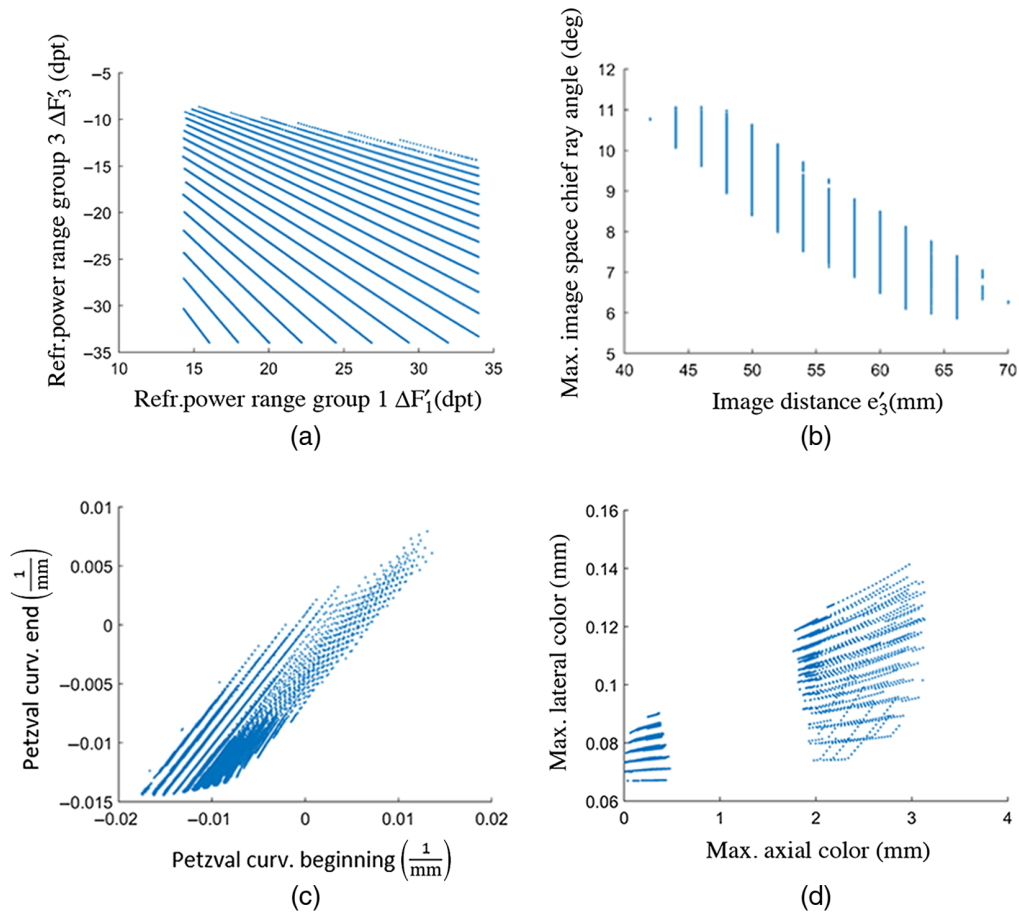\end{aligned}
\tag{5}
$$

Fig. 7 Plots of the considered first-order layouts: (a) refractive power tuning ranges; (b) after a first manual filtering step: max. image space chief ray angle and image distance; (c) after a first manual filtering step: Petzval curvature at the beginning and end of the zoom range; and (d) after a second manual filtering step: max. Lateral and axial color for the optimum combination of Abbe numbers.

Table 7 Considered optical liquids for the tunable lenses (from official Optotune ML-20-37 Zemax® model[36]).

Name	Refractive index	Abbe number
OL1224_VIS	1.2912	108.49
OL1129_VIS_NIR	1.3823	64.8
OL1114_VIS	1.3011	101.16
OL1024_UV_VIS_NIR	1.3002	105.34
OL0901_UV_VIS_NIR	1.5587	30.276

The Abbe numbers of the tunable groups are varied between 30 and 100 in four steps. The equivalent Abbe number of non-tunable group 2 is varied between negative infinity and −10, as well as positive infinity and 30 in 200 steps. For the step sizes, the reciprocal value $\frac{1}{\text{Abbe number}}$ is used. The weighting factors for axial color are set to 1 and for lateral color are set to 20. For each combination of Abbe numbers, the merit function is evaluated for each layout, and both the Abbe number combination and the axial and lateral color contributions of the layout with the lowest merit function are given as a result. The properties of the resulting layout are given in Table 8, and the layout is shown in Fig. 8.

Table 8 Properties of the resulting layout.

Property	Symbol	Value
First partial distance	e_1'	38 mm
Second partial distance	e_2'	12 mm
Third partial distance	e_3'	50 mm
Total track	L	100 mm
Focal lengths group 1	f_{1A}'	−46.3 mm
	f_{1E}'	−502.0 mm
Refractive power range group 1	$\Delta F_1'$	19.6 dpt
Focal length of group 2	f_2'	33.5 mm
Focal lengths of group 3	f_{3A}'	−341.6 mm
	f_{3E}'	−45.1 mm
Refractive power range group 3	$\Delta F_3'$	19.2 dpt
Equivalent Abbe number group 1	ν_1	64
Equivalent Abbe number group 2	ν_2	250
Equivalent Abbe number group 3	ν_3	105
Image space chief ray angles	w_A'	9.96 deg
	w_E'	10.31 deg
Aberration residuals		
Petzval curvature	$\frac{1}{r_{pA}}$	0.000228 $\frac{1}{mm}$
	$\frac{1}{r_{pE}}$	−0.000074 $\frac{1}{mm}$
Axial color	$\Delta_\lambda s_A'$	−0.00179 mm
	$\Delta_\lambda s_E'$	0.00325 mm
Lateral color	$\frac{\Delta_\lambda y_A'}{y'}$	0.00679
	$\frac{\Delta_\lambda y_E'}{y'}$	−0.00058 mm
Absolute lateral color at outmost field	$\Delta_\lambda y_A'$	0.07338 mm
	$\Delta_\lambda y_E'$	−0.00630 mm

Even for this layout, which was selected for minimum color aberrations, the absolute lateral color value at the beginning of the zoom range of about 73-μm largely exceeds the desired pixel sizes of below 5 μm (Table 3). The plot of the color aberrations of the remaining layouts for the determined optimum combination of Abbe numbers in Fig. 7(d) shows the importance of including the analysis of color aberrations into the selection of the first-order layout.

3.3 Implementation as a Thick Lens System

The previous analysis shows that even the selected optimum layout exhibits an amount of lateral color that will most likely prevent achieving the desired performance. To test the method and to get a better idea of the validity of the first-order analysis, the selected layout will nonetheless be implemented as a thick lens system in the commercial raytracing software Zemax®.
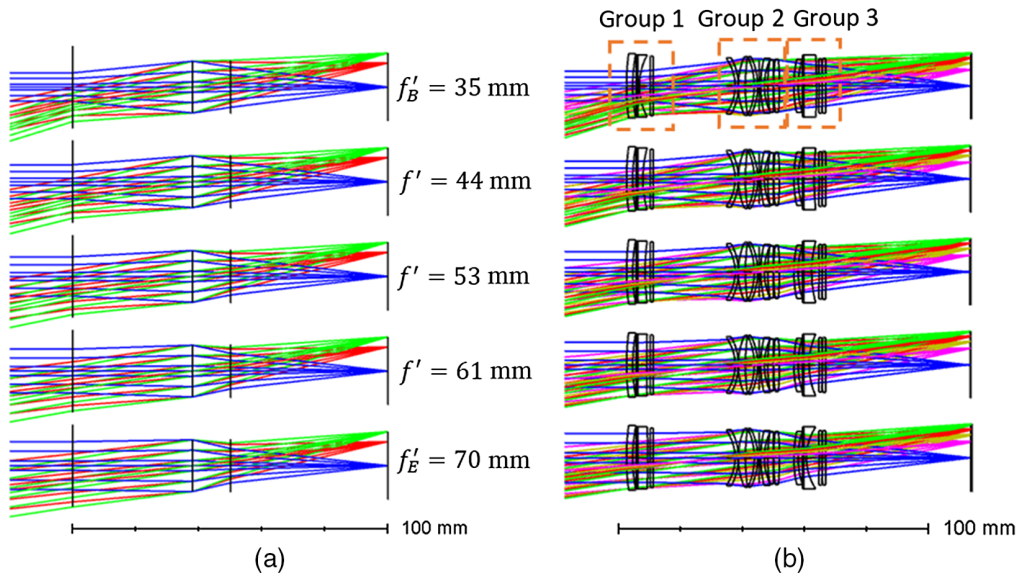
Fig. 8 (a) Chosen first-order layout and (b) first implementation as a thick lens system.

As a first step, each group is set up and pre-optimized individually for its respective equivalent Abbe number and approximate object- and image distances over the zoom range. Each of these groups is subsequently integrated into the first-order layout one after another. Small optimizations are performed to make sure the overall system works paraxially. In this step, small deviations from the calculated focal lengths of the tunable lenses are necessary to account for the axial motion of the membranes during focal length variation. This gives the first thick lens system as a starting point for the optimization algorithms of Zemax® (Fig. 8). The unaesthetic shape of the lenses resulting from the individual optimization already shows the strained state of the system.

After some optimization, including the addition of aspherical surfaces, the system arrives at a point where no further improvement is noticeable and lateral color clearly limits the performance (Fig. 9).
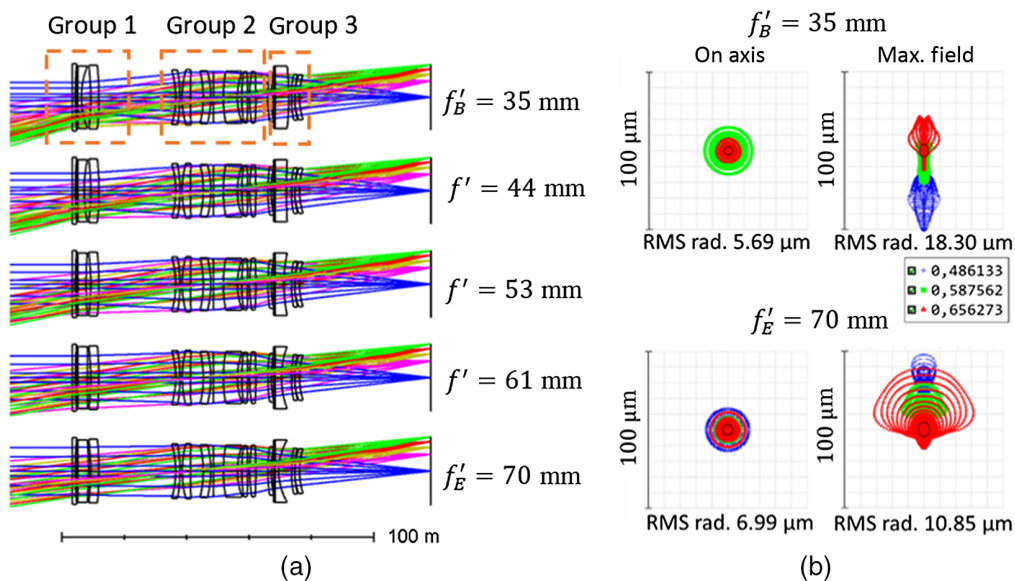

Fig. 9 (a) Slightly optimized system and (b) spot diagrams for the beginning and end of the zoom range.

Table 9 Comparison of the most important characteristics of the optimized thick lens implementation and the values calculated for the first-order layout.

Property	Symbol	First-order calculated	Optimized thick lens
Total track	L	100 mm	115 mm
Focal lengths group 1	f'_{1A}	−46.3 mm	−52.4 mm
	f'_{1E}	−502.0 mm	−468.7 mm
Refractive power range group 1	$\Delta F'_1$	19.6 dpt	17.0 dpt
Focal length of group 2	f'_2	33.5 mm	34.6 mm
Focal lengths of group 3	f'_{3A}	−341.6 mm	−230.6 mm
	f'_{3E}	−45.1 mm	−42.7 mm
Refractive power range group 3	$\Delta F'_3$	−19.2 dpt	−19.1 dpt
Image space chief ray angles	w'_A	9.96 deg	10.04 deg
	w'_E	10.31 deg	9.894 deg
Aberration residuals			
Petzval curvature	$\frac{1}{r_{pA}}$	$0.000228 \frac{1}{mm}$	$-0.001699 \frac{1}{mm}$
	$\frac{1}{r_{pE}}$	$-0.000074 \frac{1}{mm}$	$0.000102 \frac{1}{mm}$
Axial color	$\Delta_\lambda s'_A$	−0.00179 mm	−0.06906 mm
	$\Delta_\lambda s'_E$	0.00325 mm	0.11420 mm
Absolute lateral color at outmost field	$\Delta_\lambda y'_A$	0.07338 mm	0.03753 mm
	$\Delta_\lambda y'_E$	−0.00630 mm	−0.02528 mm

Table 9 gives the comparison of the most important characteristics of the final optimized thick lens system to the values calculated for the first-order layout; additional data and modulation transfer function (MTF) charts can be found in Appendix D.

Table 9 shows some differences between the values calculated based on the first-order layout and the optimized thick lens system. However, the differences are quite small when it comes to the overall performance of the system. The necessary refractive power ranges of the tunable groups are well below 20 dpt, and the image space chief ray angles have values of about 10° at the beginning and end of the zoom range and Petzval curvature is no problem, whereas lateral color is challenging. Especially when looking at the values for the color aberrations, it becomes clear that the magnitude of the difference between lateral color at the end and at the beginning of the zoom range stays quite constant: 79.68 μm for the first-order layout and 62.81 μm for the optimized thick lens system. It is also very clear that the lower lateral color value for the thick lens system is achieved by accepting a considerably higher axial color value.

4 Results and Discussion

4.1 First Conclusions

As demonstrated, the presented method allows for systematic exploration of the solution space and the selection of one specific first-order layout. The comparison between the characteristics of the thick lens systems and the values that are calculated based on the first-order layout shows that the layout's expected performance can be evaluated reasonably based on the equations presented in Sec. 2.3.

The example also demonstrates the difficulty in color correction of zoom lenses based on tunable lenses, which has already been described in Ref. 14. As also discussed in Ref. 14, for fluidic lenses, this is due to the inability of tunable groups with one single membrane lens to be color corrected over the whole tuning range. This makes the reduction of both lateral and axial color to acceptable values especially difficult. A possible solution for this problem suggested in Refs. 14 and 37 is the combination of two tunable lenses of liquids with crown- and flint-like behavior, respectively. Thereby, the tunable group can be chromatically corrected over the whole tuning range. However, as for non-tunable achromats, this also results in stronger curvatures for the same overall refractive power. For tunable doublets this reduces the available tuning range. Inserting the maximum refractive power of the tunable lens as 18 dpt, and using the liquids with the maximum Abbe number difference from Table 7 (OL1224 with $\nu_{n.\text{crown}} = 108.49$ and OL0901 with $\nu_{n.\text{flint}} = 30.276$) results in $F'_{n.\max} = 12.976$ dpt for a fully corrected doublet ($\nu_n \to \infty$). This means that the maximum refractive power range for such a doublet is $\Delta F'_{n.\max} = 25.953$ dpt. Looking back at Fig. 6, it is clear that only the systems of variation 3 can be used with the current requirements. This shows that the search for a suitable first-order layout with low requirements for the refractive power range of the tunable groups becomes even more important for such systems.

4.2 Zoom Lens with Membrane Doublets

As an example of the possibilities of systems with chromatically corrected membrane doublets, another system is created. The selection of the first-order layout is performed similarly to the example above, except from the consideration of the chromatic aberrations: because all of the groups are considered to be able to be chromatically corrected within themselves, the chromatic aberrations do not play a role in the selection of the final layout. Instead, more emphasis is put on reducing the relative aperture of the groups, to reduce the challenge of correcting the shape dependent aberrations. The selected first-order layout, as well as the optimized thick lens layout is shown in Fig. 10.

The spot diagrams and the MTF charts shown in Fig. 11 demonstrate that the color aberrations especially have been reduced considerably. Thereby the system is very close to the MTF requirements set for a 16 MP system, although it misses them by some decimal places. Apart from the improvement in color aberrations, a large step forward in correction of shape dependent aberrations (specifically spherical aberration and coma) is achieved by allowing the membrane lenses within one group to be tuned independently and by adding curvature and asphericity to the
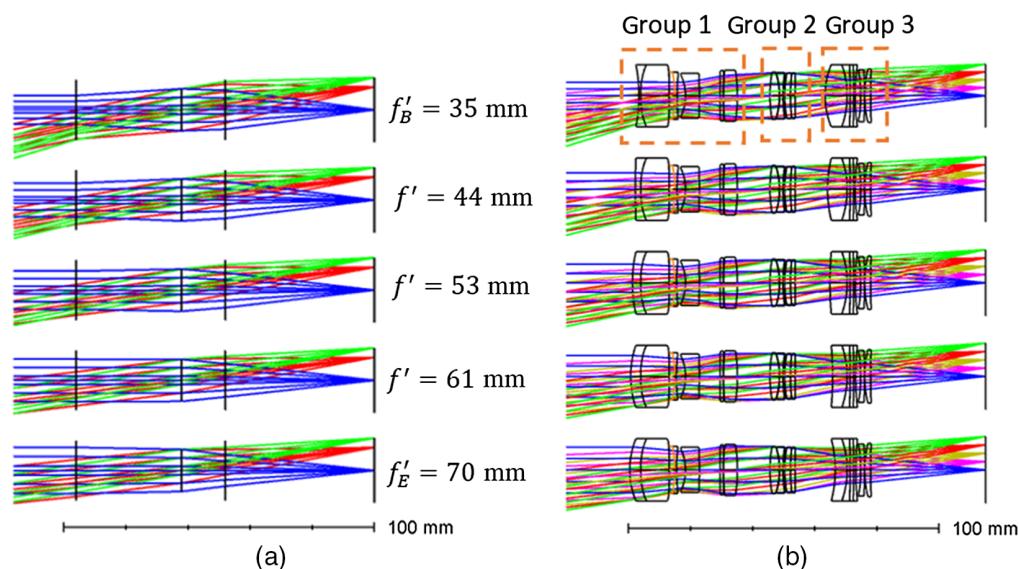

Fig. 10 (a) First-order layout and (b) optimized thick lens system for the system with membrane doublets.
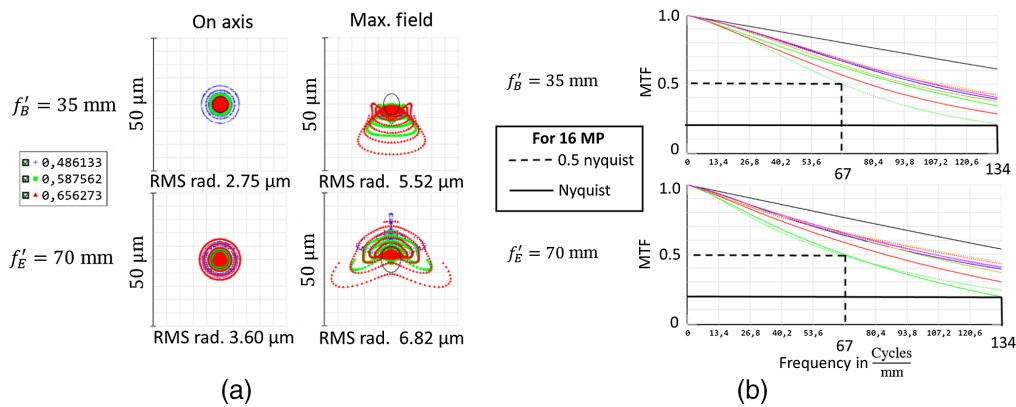
Fig. 11 (a) Spot diagrams and (b) MTF charts for the system with membrane doublets at the beginning and end of the zoom range.

cover glasses of the membrane lenses' liquid chambers. Of course, even with the improvements compared with the first design, the system cannot compete with the performance of comparable classical zoom lenses. The especially quite strong distortion (6%), low zoom ratio (2×), and long total track (115 mm), despite the large number of 19 aspherical surfaces, are critical points. Additional data for the optimized system with membrane doublets can be found in Appendix E.

4.3 Current Limitations of the Method

Despite its demonstrated usefulness, the presented method is still subject to a number of limitations: Most importantly, the direct search approach requires the processing of large amounts of data. This results in relatively long calculation times (e.g., about 7.5 h for 17 million layouts on a laptop with a 4 core 1,6 GHz i5-8250U CPU and 8 GB RAM) and limits the smallest possible step sizes. However, because the results of the solution space scan are saved and can be easily accessed and analyzed later for different sets of requirements, these long calculation times only occur once during evaluation of a certain part of the solution space. For example, the automatic prefiltering of the systems for variation 3 discussed above (Fig. 6) only requires about 0.5 h. Apart from that, the required computing time can certainly be reduced by a more efficient implementation of the program.

The other main limitation is the first-order approximation. This prevents a detailed consideration of the "shape dependent"[29] aberrations spherical aberration, coma, and astigmatism during the selection process of the final layout. Because the change of the membrane's curvature leads to strong changes in the contributions of the tunable lenses to these aberrations, these clearly pose a challenge for zoom lenses with tunable lenses.

Additionally, the presented calculation approach does not regard the change in principal plane position that results from the change of curvature in membrane lenses, unlike the equations presented in Ref. 17. As discussed for the presented example, this requires an additional optimization step of the membrane lens refractive power during thick lens design. However, the presented example demonstrates that this deviation from the calculated first-order design only leads to very small changes for the whole system. Moreover, ignoring this specific effect of membrane lenses allows the method to be applied to different tunable lens technologies and reduces the number of necessary assumptions at the beginning of the design process, e.g., on lens diameters of the final system.

4.4 Comparison with Other Zoom Lens Design Methods

As mentioned in the introduction, various similar design methods exist for classical zoom lenses. There are many examples for approaches that use advanced global search methods to fully automate the first-order design, giving the user only one or few optimum solutions.[24] These methods

are comfortable and helpful in quickly finding good solutions. However, they do not help the designer to gain an understanding of the wider solution space, making decisions about possible changes in requirements or boundary conditions more difficult.

Other methods for classical zoom lenses, specifically the ones proposed by Yee et al.[23] and Lippmann et al.,[25] do perform an analysis of the solution space and generate a large number of first-order solutions. They even include the first steps of thick lens design, which can be performed in a more standardized way for groups without tunable lenses. However, this way of estimating the aberrations of the final system conceptually requires more computational effort than the equations based on paraxial marginal and chief rays demonstrated above. The applied random variation of input parameters using Monte Carlo methods allows for statistical evaluation of the solution space. Nevertheless, this randomness also means that there are no predefined step sizes, inevitably leading to unnecessarily small step sizes in some parts of the solution space while leaving larger gaps in other parts. So, unlike the presented method, these methods do not directly lead to a mapping of the solution space, but they do give information about the solution space and provide very detailed information for selected solutions by incorporating thick lens design.

Apart from these methods for classical zoom lenses, Ref. 28 describes a design method for two element reflective telescopes based on two adaptive mirrors. The fundamental approach is very similar to the presented method, with a variation of input parameters for scanning the paraxial solution space and tracing of marginal and chief rays combined with third order aberration theory to evaluate the solutions.

5 Conclusions

The strong impact of the first-order layout for zoom lenses, combined with the relative novelty of tunable lenses, requires an approach for analyzing the solution space of zoom systems based on tunable lenses. The presented method allows one to map the first-order solution space within given boundaries and to efficiently find layouts that meet the chosen requirements. This efficiency is possible due to results from the analysis of the fundamental first-order equations; they show that there are no additional extremal points of the tunable groups' refractive power, so the layout characteristics at the beginning and end of the zoom range provide the whole tuning range.

Both the systematic, step-wise filtering of the layouts and the application of traditional thin lens aberration formula further increase the efficiency and allow for selecting the final layout based on a broad range of characteristics. The discussed example demonstrates the good agreement between these calculated characteristics and the performance of the final thick lens layout. Additionally, the example confirms the particular difficulty in correcting color aberrations in this type of zoom lenses, but it also shows how the knowledge over the surrounding solution space allows for fast and specific choice of measures for improvement of the design, which is not easily attained with existing design methods.

A remaining challenge is the transformation from the selected first-order layout to the first thick lens starting point. Design rules for this step, together with the application of the method to further, maybe more promising, examples, may form the aim of future research on the topic.

6 Appendix A: Derivation of the Calculation Approach for Variation 3

6.1 A.1 Derivation of $F_1'(F')$

The first step is based on geometric considerations and the well-known relation for the magnification β':

$$\beta' = \frac{a'}{a}, \tag{6}$$

where a is the distance from the first principal plane H to the object plane and a' the distance from the second principal plane H' of the optical system to the image plane. As we consider the

groups of our zoom lenses to be thin lenses, both principal planes will coincide for all following considerations within the calculation approach. We also use the well-known sign convention in which distances are considered positive when going from the respective principal plane with the direction of light propagation, and distances are considered negative if we move from the respective principal plane against the direction of light propagation.

From the geometry and Eq. (6), we write

$$a_4' = e_4' = \text{const.} \tag{7}$$

$$a_4 = \frac{e_4'}{\beta_4'} = a_3' - e_3', \tag{8}$$

$$0 = \beta_4' a_3' - \beta_4' e_3' - e_4'. \tag{9}$$

Now, looking at the first three groups,

$$a_3' = a_3 \beta_3', \tag{10}$$

$$a_3 = a_2' - e_2' = a_2 \beta_2' - e_2', \tag{11}$$

$$a_2 = \frac{1}{F_1'} - e_1'. \tag{12}$$

Using Eq. (12) to express a_3 within Eq. (11) and Eq. (11) to express a_3 within Eq. (10) and inserting the resulting equation into Eq. (9) to eliminate a_3', we end up with

$$0 = \beta_2' \beta_3' \beta_4' \left(\frac{1}{F_1'} - e_1' \right) - \beta_3' \beta_4' e_2' - \beta_4' e_3' - e_4'. \tag{13}$$

Another important and well-known relation describes the overall refractive power for our case of object at infinity:

$$F' = \frac{F_1'}{\beta_2' \beta_3' \beta_4'}. \tag{14}$$

This relation is used to eliminate β_4' from Eq. (13) to get the following equation, which is already independent of the second tunable group (group 4):

$$0 = \frac{F_1'}{F'} \left(\frac{1}{F_1'} - e_1' \right) - \frac{F_1'}{\beta_2' F'} e_2' - \frac{F_1'}{\beta_2' \beta_3' F'} e_3' - e_4'. \tag{15}$$

Our next aim is to express all magnifications depending on the partial distances and refractive powers of the groups. For this, we use the following well-known relation for the magnification depending on the focal length f':

$$\beta' = \frac{f'}{f' + a} \tag{16}$$

Using the refractive power instead of the focal length, we get

$$\beta' = \frac{1}{1 + aF'} = 1 - a'F'. \tag{17}$$

We use Eq. (17) to get

$$\beta_2' = \frac{1}{1 + a_2 F_2'}. \tag{18}$$

Eqs. (17) and (11) give us

$$\beta_3' = \frac{1}{1 + a_3 F_3'} = \frac{1}{1 + (a_2\beta_2' - e_2')F_3'}. \tag{19}$$

Combining Eqs. (18) and (19), we arrive at

$$\beta_2'\beta_3' = \frac{1}{\frac{1 - e_2' F_3'}{\beta_2'} + a_2 F_3'} = \frac{1}{(1 + a_2 F_2')(1 - e_2' F_3') + a_2 F_3'}. \tag{20}$$

We insert Eqs. (18) and (20) into Eq. (15) to get

$$0 = \frac{1}{F'} - \frac{F_1'}{F'}e_1' - \frac{F_1'}{F'}(1 + a_2 F_2')e_2' - \frac{F_1'}{F'}[(1 + a_2 F_2')(1 - e_2' F_3') + a_2 F_3']e_3' - e_4'. \tag{21}$$

Now, we only have to eliminate a_2 using Eq. (12). Solving for F_1' gives us the relation $F_1'(F')$ that we aimed for:

$$F_1' = \frac{e_4' F' - (1 - e_3'(F_2' - e_2' F_2' F_3' + F_3') - e_2' F_2')}{-e_1' - e_2'(1 - e_1' F_2') + e_3'(e_1'(F_2' - e_2' F_2' F_3' + F_3') - 1 + e_2' F_3')}. \tag{22}$$

6.2 A.2 Derivation of $F_4'(F_1')$

The distance between image and object L is defined as follows:

$$L = -a + a'. \tag{23}$$

Together with Eqs. (6) and (16), we write

$$f' = a'\left(1 + \frac{a'}{L}\right). \tag{24}$$

Applied to group 4, this gives us

$$F_4' = \frac{1}{a_4'\left(1 - \frac{a_4'}{L_4}\right)}. \tag{25}$$

Geometry gives us

$$L_4 = L - e_1' - e_2' - a_3' = e_3' + e_4' - a_3'. \tag{26}$$

We use Eqs. (10) and (17) to express a_3' depending on a_3:

$$a_3' = \frac{a_3}{1 + a_3 F'} = \frac{1}{\frac{1}{a_3} + F_3'}. \tag{27}$$

Inserting Eqs. (17) into (11) gives us a_3 depending on a_2:

$$a_3 = \frac{1}{\frac{1}{a_2} + F_2'} - e_2'. \tag{28}$$

From this point, we only need to insert Eq. (12) into Eq. (28), the result into Eq. (27), and this into Eq. (26). Inserting this into Eq. (25) gives us our relation $F_4'(F_1')$:

$$F_4' = \frac{1}{e_4' \left(1 - \frac{e_4'}{e_3' + e_4' - \frac{1}{\frac{1}{\frac{1}{F_1' - e_1'} + F_2'} - e_2'} + F_3'}} \right)}. \tag{29}$$

7 Appendix B: Derivation of the Derivative of $F_4'(F_1')$

At first, we need the first derivative of $F_4'(F_1')$. To make the calculations more convenient, we start with a slightly different writing of Eq. (25):

$$F_4'(F_1') = \frac{1}{a_4' \left(1 - \frac{a_4'}{L_4(F_1')} \right)} = \frac{1}{a_4'} (1 - a_4'(L_4(F_1'))^{-1})^{-1}. \tag{30}$$

The first derivative of this is

$$\frac{\delta F_4'}{\delta F_1'} = -\frac{1}{a_4'} \left(1 - \frac{a_4'}{L_4(F_1')} \right)^{-2} \cdot (-1) \cdot a_4'(L_4(F_1'))^{-2} \frac{\delta L_4(F_1')}{\delta F_1'} \tag{31}$$

Now, we focus on the $\frac{\delta L_4(F_1')}{\delta F_1'}$ part. Looking back at Eq. (26) shows that the object to image distance for group 4 depending on F_1' can be written as

$$L_4 = e_3' + e_4' - a_3'(F_1'). \tag{32}$$

Because the partial distances e_3' and e_4' do not change over the zoom range, it is clear that

$$\frac{\delta L_4(F_1')}{\delta F_1'} = \frac{\delta a_3'(F_1')}{\delta F_1'}. \tag{33}$$

Using the relations Eqs. (6) and (17), $a_3'(F_1')$ is expressed as

$$a_3'(F_1') = \frac{1}{\frac{1}{a_3(F_1')} + F_3'} = ((a_3(F_1'))^{-1} + F_3')^{-1}. \tag{34}$$

The first derivative of this is

$$\frac{\delta a_3'(F_1')}{\delta F_1'} = -((a_3(F_1'))^{-1} + F_3')^{-2} \cdot (-1) \cdot (a_3(F_1'))^{-2} \frac{\delta a_3(F_1')}{\delta F_1'}. \tag{35}$$

So, we can focus on $a_3(F_1')$, which according to Eq. (28) is

$$a_3(F_1') = \frac{1}{\frac{1}{a_2(F_1')} + F_2'} - e_2' = ((a_2(F_1'))^{-1} + F_2')^{-1} - e_2', \tag{36}$$

and its first derivative, which is

$$\frac{\delta a_3(F_1')}{\delta F_1'} = -((a_2(F_1'))^{-1} + F_2')^{-2} \cdot (-1) \cdot (a_2(F_1'))^{-2}\frac{\delta a_2(F_1')}{\delta F_1'}. \tag{37}$$

$a_2(F_1')$ is known from relation Eq. (12), and its first derivative is

$$\frac{\delta a_2(F_1')}{\delta F_1'} = -(F_1')^{-2}. \tag{38}$$

Putting Eqs. (31), (33), (35), (37), and (38) together finally gives us

$$\frac{\delta F_4'}{\delta F_1'} = -(L_4(F_1') - a_4')^{-2} \cdot ((a_3(F_1'))^{-1} + F_3')^{-2}$$
$$\cdot (a_3(F_1'))^{-2}((a_2(F_1'))^{-1} + F_2')^{-2} \cdot (a_2(F_1'))^{-2}(F_1')^{-2}. \tag{39}$$

8 Appendix C: Lateral Color: Factor *c* for the Aperture Stop Positions in the First Three Groups

As shown in Fig. 12, the factor c describes the relative position of the entrance pupil to the first group of the system and the object as[30]
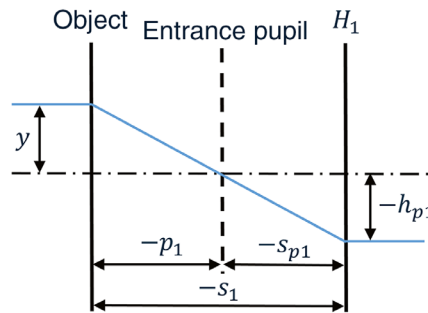

Fig. 12 Geometry for factor c.[30]

$$c = -\frac{s_1 s_{p1}}{p_1} = \frac{1}{\left(\frac{1}{s_1} - \frac{1}{s_{p1}}\right)}. \tag{40}$$

Concerning the signs of the distances, it has to be noted that the reference point for p_1 is the entrance pupil, whereas for s_1 and s_{p1}, it is the first principal plane of the first group H_1. If c is to be expressed depending on the known system properties, it has to be performed depending on the position of the aperture stop. In the following, the expressions will be given for an aperture stop within one of the first three groups of the system.

8.1 *C.1 Aperture Stop within Group 1:*

Here the first group does not influence pupil imaging. Because lateral color is caused by axial color of pupil imaging, clearly the first group is not directly contributing to this. The equation has to be applied only to the last three groups of the system. The intermediate image of the object, produced by the first group, is considered to be the object. With that, the distances in Eq. (40) are expressed as

$$s_1 = -(e_1' - f_1'), \tag{41}$$

$$s_{p1} = -e'_1, \tag{42}$$

$$p_1 = f'_1. \tag{43}$$

The factor c becomes

$$c = -(F'_1 e'^2_1 - e'_1). \tag{44}$$

8.2 *C.2 Aperture Stop within Group 2:*

Here the equation is applied to the whole system, and we get

$$s_1 = -\infty. \tag{45}$$

Using the well-known equation

$$F' = \frac{1}{a'} - \frac{1}{a}, \tag{46}$$

we get

$$F'_1 = \frac{1}{e'_1} - \frac{1}{s_{p1}}. \tag{47}$$

The factor c becomes

$$c = -\frac{1}{\frac{1}{e'_1} - F'_1}. \tag{48}$$

8.3 *C.3 Aperture Stop within Group 3*

Here, the entrance pupil is the image of the aperture stop, produced by group 1 and 2. Using Eq. (46),

$$F'_2 = \frac{1}{e'_2} - \frac{1}{s_{p2}}, \tag{49}$$

$$F'_1 = \frac{1}{e'_1 + s_{p2}} - \frac{1}{s_{p1}}. \tag{50}$$

The factor c is expressed as

$$c = -\frac{1}{\frac{1}{e'_1 + \frac{1}{\frac{1}{e'_2} - F'_2}} - F'_1}. \tag{51}$$

9 Appendix D: Data for the First Optimized Thick Lens System

9.1 *D.1 Surface data*

Tables 10 and 11 show the surface data and the variable membrane radii and corresponding focal lengths of the membrane lenses for the first optimized thick lens system, respectively

Table 10 Surface data for the optimized thick lens system. Type: A—aspherical, S—spherical, M—membrane, STOP-aperture stop, and IMA-image plane. The thicknesses at the surface before a membrane surface and the membrane itself are measured with respect to the membrane with zero curvature. The radii for the membranes for five zoom positions are shown in Table 11; aspherical surfaces are even aspheres described by the typical sag equation used in ZEMAX®: $z = \frac{cr^2}{1+\sqrt{1-(1+k)c^2r^2}} + A_1 r^2 + A_2 r^4 + A_3 r^6 + A_4 r^8 + \dots$ (c-surface curvature, k-conic constant, A_n-aspheric coefficient). Note that, due to the limited number of digits, the values from this table do not directly yield a system with the performance discussed in the paper; a little bit of reoptimization is necessary.

| No. | Type | Radius (mm) | Thick. (mm) | Cl. Sem. diam. (mm) | Material | Aspheric coefficients | | | |
						Second-order (mm^{-1})	Fourth-order (mm^{-3})	Sixth-order (mm^{-5})	Eighth-order (mm^{-7})
1	A	588.363	1.000	10.739	N-BK7	3.901E−4	−4.449E−7	−6.409E−8	1.898E−10
2	S	130.810	0.383	10.560	—	—	—	—	—
3	S	Inf	0.500	10.000	N-BK7	—	—	—	—
4	S	Inf	3.000	10.000	OL1129	—	—	—	—
5	M	Table 11	1.080	10.000	—	—	—	—	—
6	A	−80.150	2.619	10.212	N-BK7	−5.657E−4	4.781E−6	8.162E−8	−2.643E−10
7	S	−112.481	24.628	10.044	—	—	—	—	—
8	A	−31.853	1.373	8.515	N-LAK33B	8.491E−5	−9.020E−6	−6.968E−8	3.618E−10
9	S	−51.068	0.716	8.702	—	—	—	—	—
10	S	33.424	2.663	8.834	N-LAK33B	—	—	—	—
11	S	247.696	4.096	8.691	—	—	—	—	—
12	A	−35.476	2.428	8.321	N-SF66	7.780E − 5	-9.513E − 7	1.315E − 8	-1.180E − 10
13	A	−33.814	0.874	8.454	—	−7.327E − 5	5.777E−7	−6.134E−9	1.350E−10
14	STOP	Inf	3.156	8.200	—	—	—	—	—
15	S	46.410	4.500	8.367	N-SF66	—	—	—	—
16	A	24.284	1.384	8.031	—	1.608E−3	−1.138E−8	−2.555E−8	−9.506E−10
17	S	55.160	1.924	8.144	N-LAK33B	—	—	—	—
18	S	−151.158	0.624	8.201		—	—	—	—
19	S	52.543	1.972	8.276	N-LAK33B	—	—	—	—
20	A	−151.877	3.875	8.232	—	−4.660E−5	−9.630E−6	5.708E−8	1.016E−9
21	S	54.534	1.000	7.754	N-BK7	—	—	—	—
22	S	33.639	0.870	7.600		—	—	—	—
23	S	Inf	0.500	10.000	N-BK7	—	—	—	—
24	S	Inf	3.800	10.000	OL1024	—	—	—	—
25	M	Table 11	1.389	10.000	—	—	—	—	—
26	A	39.603	1.019	7.311	N-SF5	−2.670E−4	4.861E−6	1.949E−7	6.834E−10
27	S	28.440	0	7.191		—	—	—	—
28	S	20.686	1.578	7.218	N-BK7	—	—	—	—
29	A	29.109	42.051	7.112		2.343E−3	2.411E−5	1.148E−7	1.466E−9
30	IMA	Inf	—	—	—	—	—	—	—

Table 11 Radii of the membranes and focal lengths of the membrane lenses in mm for five zoom positions (configurations) for the optimized thick lens system.

Surface No.	System focal length in mm				
	35	43.75	52.5	61.25	70
	Radii of membranes in mm				
5	27.306	49.929	120.595	−1813.263	−131.276
25	−94.949	211.661	49.838	28.349	19.898
	Focal lengths of membrane lenses in mm				
3–5	−71	−131	−315	4743	343
23–25	316	−705	−166	−94	−66

9.2 *D.2 MTF Charts*

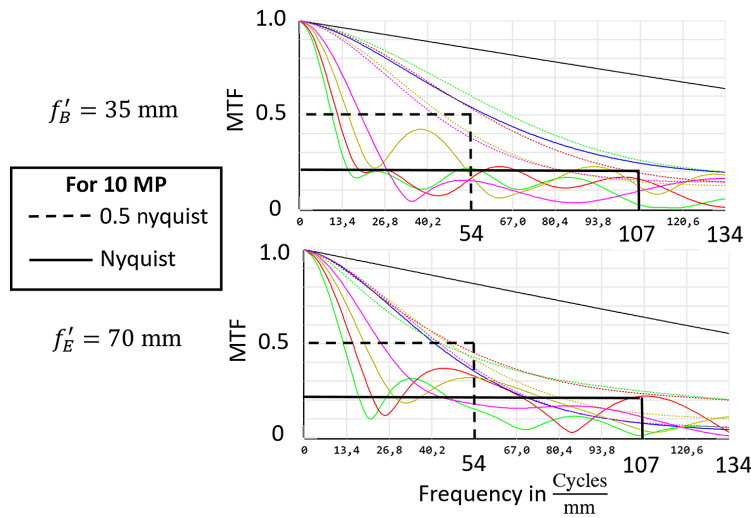Figure 13 shows the MTF charts of the first optimized thick lens system.

Fig. 13 MTF charts for the optimized thick lens system at both ends of the zoom range.

10 Appendix E: Surface Data for the Optimized Thick lens System with Membrane Doublets

Table 12 contains the surface data for the optimized thick lens system with membrane doublets, and Table 13 shows the variable membrane radii, the stop diameters as well as the focal lengths of the membrane lenses. It is obvious that the membrane doublets no longer are chromatically corrected within themselves over the whole tuning range after allowing the membranes to vary their curvature independently during optimization. This can be explained by the need to reduce shape dependent aberrations. Figure 14 shows the remaining aberrations as wavefront aberrations at the beginning, in the middle, and at the end of the zoom range both on axis and for the maximum field.

Table 12 Surface data for the optimized thick lens system with membrane doublets. Type: A—aspherical, S—spherical, and M—membrane. The thicknesses at the surface before a membrane surface and the membrane itself are measured with respect to the membrane with zero curvature. The radii for the membranes for five zoom positions are shown in Table 13; aspherical surfaces are even aspheres described by the typical sag equation used in ZEMAX®: $z = \frac{cr^2}{1+\sqrt{1-(1+k)c^2r^2}} + A_1 r^2 + A_2 r^4 + A_3 r^6 + A_4 r^8 + \ldots$ (c-surface curvature, k-conic constant, and A_n-aspheric coefficient). Note that, due to the limited number of digits, the values from this table do not directly yield a system with the performance discussed in the paper; a little bit of reoptimization is necessary.

No.	Type	Radius (mm)	Thick. (mm)	Cl. Sem. diam. (mm)	Material	Aspheric coefficients				
						Second-order (mm^{-1})	Fourth-order (mm^{-3})	Sixth-order (mm^{-5})	Eighth-ord. (mm^{-7})	Tenth-ord. (mm^{-9})
1	M	Table 13	1.515	10.000	OL1024	—	—	—	—	—
2	A	69.609	9.190	10.000	N-BK7	6.842E−3	3.794E−5	1.117E−7	−1.232E−10	—
3	A	−497.705	0.000	10.000		−2.701E−4	−2.537E−6	8.191E−8	−5.162E−9	—
4	A	624.417	1.821	7.588	P-LAK35	2.259E−4	1.006E−6	−1.268E−7	2.104E−9	—
5	A	−6715.340	1.452	7.382	OL0901	−0.011	−4.126E−5	−1.608E−6	3.146E−8	—
6	M	Table 13	1.991	7.029	—	—	—	—	—	—
7	A	−17.479	4.464	6.799	N-LAF2	−2.587E−3	−1.528E−5	−2.611E−7	9.779E−10	—
8	S	−183.463	6.693	7.237	—	—	—	—	—	—
9	S	527.947	1.048	7.963	N-LAF2	—	—	—	—	—
10	S	529.841	0.017	8.029	—	—	—	—	—	—
11	S	80.533	4.500	8.073	EP-7000	—	—	—	—	—
12	A	−53.516	10.473	8.183	—	−8.883E−6	−2.130E−7	−1.265E−8	2.143E−10	—
13	A	45.473	3.033	7.590	N-LAK33B	7.955E−4	−4.492E−6	−2.594E−8	−1.737E−10	—
14	S	−24.367	0.125	7.471	—	—	—	—	—	—

Table 12 (*Continued*).

No.	Type	Radius (mm)	Thick. (mm)	Cl. Sem. diam. (mm)	Material	Aspheric coefficients				
						Second-order (mm⁻¹)	Fourth-order (mm⁻³)	Sixth-order (mm⁻⁵)	Eighth-ord. (mm⁻⁷)	Tenth-ord. (mm⁻⁹)
15	A	−23.626	0.999	7.429	SF4	$-1.831E{-}4$	$-6.967E{-}6$	$1.055E{-}7$	$-1.636E{-}10$	—
16	S	48.090	0.599	7.172	—	—	—	—	—	—
17	STOP	Inf	0.000	Table 13	—	—	—	—	—	—
18	A	38.129	1.862	7.310	SF57HTULTRA	$-3.785E{-}5$	$8.025E{-}6$	$-1.042E{-}7$	$8.912E{-}10$	—
19	A	70.405	0.000	7.320	—	$1.118E{-}4$	$-4.606E{-}6$	$-4.612E{-}8$	$6.747E{-}10$	—
20	S	59.462	1.466	7.328	N-SSK2	—	—	—	—	—
21	S	1036.621	11.654	7.342	—	—	—	—	—	—
22	M	Table 13	5.114	10.000	OL1024	—	—	—	—	—
23	A	−57.025	0.999	10.000	N-BK7	$-7.277E{-}3$	$-2.650E{-}5$	$9.302E{-}8$	$6.980E{-}10$	—
24	A	−178.632	0.000	10.000	—	$4.251E{-}4$	$-4.311E{-}6$	$-2.876E{-}8$	$1.987E{-}9$	—
25	A	−171.554	1.028	10.000	N-BK7	$-5.112E{-}4$	$7.207E{-}6$	$8.213E{-}8$	$8.946E{-}10$	—
26	A	2140.717	1.273	10.000	OL0901	$-3.592E{-}4$	$1.032E{-}5$	$-1.423E{-}7$	$-7.502E{-}10$	—
27	M	Table 13	1.070	10.000	—	—	—	—	—	—
28	A	−66.991	1.256	8.045	SF10	$-2.31E{-}3$	$-2.240E{-}5$	$-1.541E{-}7$	$1.177E{-}9$	—
29	S	−155.404	0.000	8.302	—	—	—	—	—	—
30	A	40.079	1.911	8.574	N-LAF33	$1.749E{-}3$	$-4.042E{-}6$	$4.136E{-}8$	$5.034E{-}10$	—
31	A	202.218	36.961	8.571	—	$-8.054E{-}5$	$-4.474E{-}6$	$5.990E{-}10$	$1.587E{-}9$	$-4.697E{-}12$
32	IMA	Inf	—	—	—	—	—	—	—	—

Table 13 Radii of the membranes, semi diameter of the aperture stop, and focal lengths of the membrane lenses in mm for five zoom positions (configurations) for the optimized thick lens system with membrane doublets. Note the different orientations of the membranes (6 and 27 are oriented in the opposite direction of 1 and 22). Therefore, same signs of the radius do not necessarily mean the same sign of the resulting refractive power.

| Surface No.	System focal length in mm				
	35	43.75	52.5	61.25	70
	Radii of the membranes in mm				
1	−51.520	244.817	44.637	30.203	26.057
6	72.511	70.226	56.239	52.598	55.798
22	26.231	42.859	116.475	−117.626	−40.153
27	68.403	69.482	75.538	89.068	93.846
	Aperture stop semi diameter in mm				
17	7.170	7.166	7.085	7.090	7.142
	Focal lengths of the membrane lenses in mm				
1–3	632	117	72	59	54
4–6	−297	−277	−179	−159	−176
22–24	138	376	−537	−141	−83
25–27	−85	−86	−91	−102	−105
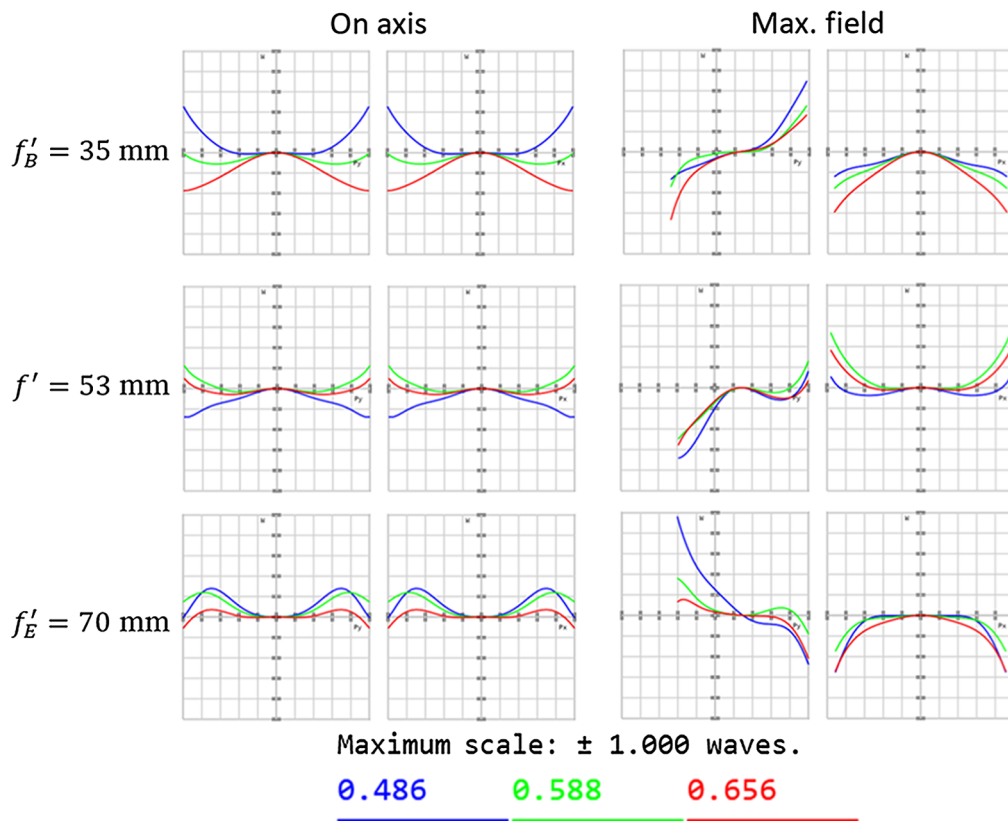
Fig. 14 Wavefront aberrations (optical path difference = OPD) for the optimized thick lens system with membrane doublets.

Acknowledgments

References

1. H. Ren and S.-T. Wu, *Introduction to Adaptive Lenses*, John Wiley & Sons, Inc., Hoboken, New Jersey (2012).
2. S. Sinzinger, "Diffractive and refractive microoptics," in *Comprehensive Microsystems*, Y. Gianchandani, O. Tabata, and H. Zappe, Eds., Elsevier, Oxford (2007).
3. H. Zappe and C. Duppe, Eds., *Tunable Microoptics*, Cambridge University Press, Cambridge UK (2016).
4. K. Mishra et al., "Optofluidic lens with tunable focal length and asphericity," *Sci. Rep.* **4**, 6378 (2014).
5. Corning Incorporated, "Corning varioptic lenses," https://www.corning.com/emea/de/innovation/corning-emerging-innovations/corning-varioptic-lenses/variable-focus-lenses-a-series.html (accessed 2 Nov. 2021).
6. Holochip Corporation, "Variable focus lenses," https://www.holochip.com/photonics (accessed 02 Nov. 2021).
7. Optotune Switzerland AG, "Focus tunable lenses," https://www.optotune.com/focus-tunable-lenses (accessed 02 Nov. 2021).
8. P. Zhao, Ç. Ataman, and H. Zappe, "Gravity-immune liquid-filled tunable lens with reduced spherical aberration," *Appl. Opt.* **55**, 7816–7823 (2016).
9. L. W. Alvarez, "Two-element variable-power spherical lens," U.S. patent 3,305,294 (1967).
10. A. W. Lohmann, "A new class of varifocal lenses," *Appl. Opt.* **9**, 1669–1671 (1970).
11. A. Grewe, M. Hillenbrand, and S. Sinzinger, "Aberration analysis of optimized Alvarez–Lohmann lenses," *Appl. Opt.* **53**, 7498–7506 (2014).
12. S. Bernet and M. Ritsch-Marte, "Adjustable refractive power from diffractive Moiré elements," *Appl. Opt.* **47**, 3722–3730 (2008).
13. A. Grewe, P. Fesser, and S. Sinzinger, "Diffractive array optics tuned by rotation," *Appl. Opt.* **56**, A89–A96 (2017).
14. F. C. Wippermann et al., "Mechanically assisted liquid lens zoom system for mobile phone cameras," *Proc. SPIE* **6289**, 62890T (2006).
15. S. C. Park and W. S. Lee, "Design and analysis of a one-moving-group zoom system using a liquid lens," *J. Korean Phys. Soc.* **62**, 435–442 (2013).
16. M. Aschwanden et al., "Optical zoom lens with two liquid lenses," U.S. patent US20160202455A1 (2016).
17. S.-H. Jo and S.-C. Park, "Design and analysis of an 8x four-group zoom system using focus tunable lenses," *Opt. Express* **26**, 13370–13382 (2018).
18. E. C. Tam, "Smart electro-optical zoom lens," *Opt. Lett.* **17**, 369–371 (1992).
19. D. V. Wick and T. Martinez, "Adaptive optical zoom," *Opt. Eng.* **43**(1), 1–2 (2004).
20. B. E. Bagwell et al., "Active zoom imaging for operationally responsive space," *Proc. SPIE* **6467**, 64670D (2007).
21. M. Quintavalla et al., "High quality adaptive optics zoom with adaptive lenses," *Proc. SPIE* **10502**, 105021H (2018).
22. A. Miks and J. Novak, "Paraxial analysis of zoom lens composed of three tunable-focus elements with fixed position of image-space focal point and object-image distance," *Opt. Express* **22**, 27056–27062 (2014).
23. A. J. Yee et al., "New tools for finding first-order zoom lens solutions and the analysis of zoom lenses during the design process," *Proc. SPIE* **9580**, 958006 (2015).
24. Z. Fan et al., "Automatically retrieving an initial design of a double-sided telecentric zoom lens based on a particle swarm optimization," *Appl. Opt.* **58**, 7379–7386 (2019).

25. D. H. Lippman, D. S. Teverovsky, and J. L. Bentley, "Monte Carlo first-order design method for anamorphic cinema zoom lenses," *Opt. Eng.* **60**(5), 051203 (2021).

26. L. Lenk, B. Mitschunas, and S. Sinzinger, "Zoom systems with tuneable lenses and linear lens movements," *J. Eur. Opt. Soc.-Rap. Publ.* **15**, 9 (2019).

27. L. Lenk, B. Mitschunas, and S. Sinzinger, "Zoom systems based on tunable lenses: a systematic first order design method," in *Paper presented at EOSAM 2021*, Rome (2021).

28. M. E. Jungwirth, D. V. Wick, and E. L. Dereniak, "Theory and tradespace analysis of a reflective axial adaptive optical zoom system," *Opt. Eng.* **51**(8), 083001 (2012).

29. M. J. Kidger, *Fundamental Optical Design*, SPIE Press, Bellingham, Washington (2001)

30. H. Haferkorn, Bewertung optischer Systeme, VEB Deutscher Verlag der Wissenschaften, Berlin (1986).

31. The Mathworks Inc., "Object oriented programming in MATLAB," https://de.mathworks.com/products/matlab/object-oriented-programming.html (accessed 2 Nov. 2021).

32. B. Kirchheim, "Testbericht: Panasonic Lumix G Vario 35-100 mm 4-5.6 Asph. O.I.S.," digitalkamera.de, 2014, https://www.digitalkamera.de/Zubeh%C3%B6r-Test/Testbericht_Panasonic_Lumix_G_Vario_35-100_mm_4-5_6_Asph_O_I_S/9222.aspx (accessed 2 Nov. 2021).

33. Digitalkamera.de, "Olympus E-450 Datenblatt," https://www.digitalkamera.de/Kamera/Olympus/E-450.aspx (accessed 02. Nov. 2021).

34. Wikipedia, "Micro four thirds system," https://en.wikipedia.org/wiki/Micro_Four_Thirds_system (accessed 2 Nov. 2021).

35. ePHOTOzine, "Complete guide to image sensor pixel size," 2016, https://www.ephotozine.com/article/complete-guide-to-image-sensor-pixel-size-29652 (accessed 2 Nov. 2021).

36. Optotune Switzerland AG, "ML-20-37-lens," https://www.optotune.com/ml-20-37-lens (accessed 2 Nov. 2021).

37. F. Santiago et al., "Large aperture adaptive doublet polymer lens for imaging applications," *J. Opt. Soc. Am. A* **31**, 1842–1846 (2014)

Leonhard Lenk has been a PhD student at the Optical Engineering Group of the Technical University of Ilmenau, Germany, since 2018. He received his BS and MS degrees in mechanical engineering in 2016 and 2018, respectively. His research interests include optical system design and both refractive and diffractive tunable lenses.

Beate Mitschunas was part of the Optical Engineering Group at the Technical University of Ilmenau for more than 30 years until her retirement in 2022. In 1985, she received her doctorate in technical optics from the department of technical optics at the Technical University of Ilmenau with Professor Haferkorn. She has been involved primarily in optical design since 1994. Her specialty is finding collinear layouts for more complex optical systems, especially zoom systems.

Stefan Sinzinger is a professor in Technische Optik (optical engineering) at the Technische Universität Ilmenau, Germany. He received his PhD from Friedrich-Alexander-Universität Erlangen-Nürnberg in 1993 and his habilitation degree from FernUniversität Hagen in 2001. As coauthor of the textbook microoptics, his research interests focus on design and fabrication of microoptical elements as well as microoptical systems integration.